20th Australasian Fluid Mechanics Conference
Perth, Australia
5-8 December 2016

Numerical Investigation of a Horizontal Axis Tidal Turbine

O. Afshar[1], A. D. Henderson[1], J. M. Walker[2], X. Wang[1]

[1]School of Engineering & ICT, University of Tasmania, Hobart, TAS 7001, Australia
[2]National Centre for Maritime Engineering & Hydrodynamics, Australian Maritime College, University of Tasmania, Launceston, Tasmania, 7248, Australia

Abstract

Horizontal Axis Tidal Turbines (HATTs) are one of the most promising technologies available for power generation from tidal energy. In this study, the performance of a twin bladed HATT based on a NACA63-618 cross-section was numerically studied using a Reynolds Averaged Navier-Stokes (RANS) solver with k-ω turbulence model. The power and thrust coefficients at different tip speed ratios were calculated and validated using previously published experimental data. Simulation results indicated that the maximum efficiency of the tidal turbine is approximately 40%, occurring at a tip speed ratio of 6. The pressure distribution at three different sections of the blade span was investigated for three values of tip speed ratio. Boundary layer separation is evident on the suction surface towards the root of the blade section at a tip speed ratio of 5. As tip speed ratio is increased to 7, the separation does not occur.

Introduction

Among sources of renewable energy, tidal stream energy has many attractive features as a clean energy resource. It is a sizable resource, distributed along coastlines and is considered to be one of the most promising energy sources [1]. The power generated from tidal turbines is more predictable than from solar and wind. Harnessing tidal power has a positive impact on climate change because it produces no greenhouse gas emissions.

Horizontal Axis Tidal Turbines operate using the lift principle and the rotor blades are commonly designed using aerodynamic section data. However, the flow fields encountered by HATT turbine blades are complex and difficult to predict [2-4]. Turbine performance is affected by factors such as turbulence and surface roughness. Many studies have been done to understand the effects of flow separation and stall on aerofoil surfaces. Johari et al [5] experimentally investigated the hydrodynamic loading of a smooth NACA634-012 aerofoil with leading-edge protuberances. The results indicated that separation originated primarily from the troughs between adjacent protuberances and the flow was attached on the peaks of the protuberances at the angles beyond the stall angle of the baseline foil. In a separate study Li et al [6] experimentally investigated the effect of turbulent inflows on the aerofoil performance of HAT at low Reynolds numbers. In order to observe the stall phenomenon, pressures on the rotor surface were measured by a multiport pressure device. In addition, static turbulence grids were used to adjust the turbulence intensity. It was found that the flow was separated at the leading edge in the case of without grids. In the case of turbulent flow field (with grid), the separated flow region expanded gradually with increasing angle of attack. Yu et al [7] paid close attention to flow separation for a HAT at different flow speeds and different span sections along the blade using 3-D CFD computations. The results showed that for most spanwise locations, the pressure coefficient was in good agreement with the experimental data, however at high flow speed the CFD results deviated from the experimental data at the mid span location. This is mainly due to the relative large flow separation and 3-D spanwise flow over the suction surface of the blade. Lee et al [8] measured velocity fields using Particle Image Velocimetry (PIV) and also conducted the static pressure measurements on the suction surfaces of static aerofoil and rotating blade. For the static aerofoil, chord wise surface pressures were flat at stall with large angles of attack. However, higher values of pressure coefficient or lower static pressures were obtained on the suction surface of the rotating blade. These studies show that the flow around HATs is complex and further research is required to improve understanding of turbine performance.

This paper describes a numerical study of a tidal turbine using a commercial Computational Fluid Dynamics (CFD) package, ANSYS 15. The numerical results are validated against experimental results that were carried out on two-bladed Horizontal Axis Tidal Turbine (HATT) with smooth blades in a 116 m long towing tank by Walker et al [9]. In addition, the relationship between the tip speed ratio and surface pressure distributions on the rotor is investigated.

Hydrodynamic Performance of Turbine

Since turbines convert the energy of a free flowing fluid to mechanical power, their performance can be evaluated by calculating the energy conversion efficiency. The turbine power characteristic is affected by factors including the current speed, turbine size and rotational speed. The power and thrust coefficients of a HATT are defined using Equations 1-2. The tip speed ratio is dimensionless value representing the ratio of the rotational speed to the inflow velocity, as shown in Equation 3. The pressure coefficient around the aerofoil can be defined using Equation 4.

$$C_P = \frac{Q\omega}{0.5\rho A U_\infty^3} \quad (1)$$

$$C_T = \frac{T}{0.5\rho A U_\infty^2} \quad (2)$$

$$\lambda = \frac{R\omega}{U_\infty} \quad (3)$$

$$C_{press} = \frac{p - p_0}{0.5 * \rho U_\infty^2} \quad (4)$$

where Q and T are the torque and thrust force, respectively, ρ is the density, A is turbine blade swept area, U_∞ is free stream velocity, ω is the rotational speed, p is the local static pressure, p_0 is the static pressure and R is the blade radius.

Turbine Model Geometry

The HATT turbine studied in this paper consisted of a two-bladed rotor with a diameter of 0.8 m. This is representative of a 1/25th scale model of a full size marine current turbine. The rotor blades of the turbine are based on a NACA63-618 aerofoil cross section. The blade geometry is detailed by Walker et al [9]. Point

coordinates required to visualize a 3-D model were obtained and the frameworks were plotted as shown in Figures 1 and 2.

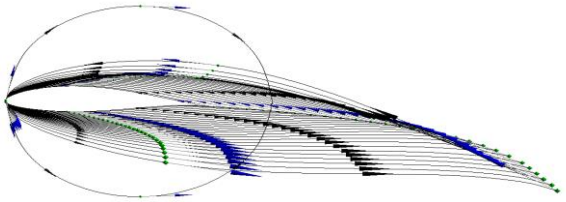

Figure 1: framework of the blade

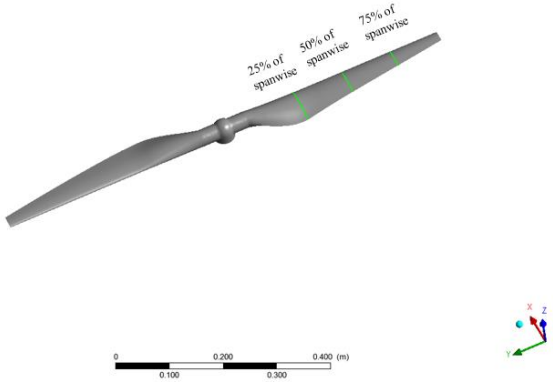

Figure 2: solid 3D model of tidal turbine blades

Boundary Conditions

Numerical analysis based on 3-D Reynolds-averaged Navier-Stokes (RANS) equations has been widely used for the flow analysis of turbo-machinery, greatly reducing the time and cost associated with experimental testing. A CFD analysis was conducted to estimate the performance of the turbine. The ANSYS CFX commercial CFD code (version 15.0) was used for the simulations, focusing on the turbine located in the analysis domain.

The analysis field was assumed to be incompressible, three dimensional, and steady state. The analysis field was composed of two domains: an internal rotating domain encompassed the blades, and an outer domain covered the remaining area of the flow channel, as shown in Figure 3.

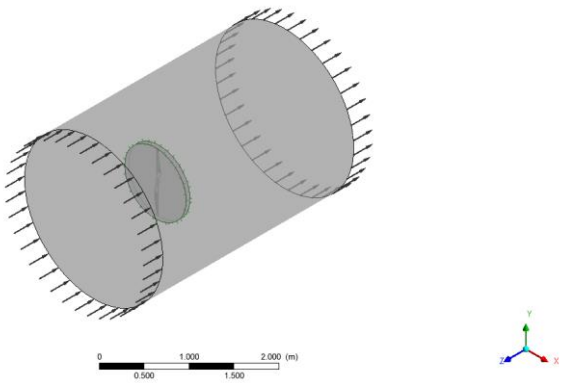

Figure 3: Computational domain for performance analysis

The outer stationary domain area used an opening condition that was similar to the environment of the towing tank. The hub and turbine blades were represented by a wall condition with non-slip surface. In addition, blockage ratio that is defined as the ratio of the rotor swept area to the external domain cross-sectional area, is approximately 0.1. A uniform normal velocity was applied to the inlet for various cases. A speed of 1.68 m/s was chosen to match the experimental condition [9]. In the rotating domain, the rotation velocity and upstream velocity are linked by tip speed ratios. As the inlet velocity is constant, the angular velocity can be adjusted to the tip speed ratio and estimated by equation 3 in the range of $5<\lambda<10$. The surfaces between the two domains were interfaced using the general grid interface method. The turbulence model performed analysis by considering the steady flow field around the aerofoil using the k-ω model. The k-ω model is well regarded for predicting the size and onset of flow separation in an adverse pressure gradient. Table 1 shows the defined boundary conditions.

Table 1: Boundary conditions

Description	Analysis condition
Working fluid	Water (isothermal, 25°C)
Inlet	Velocity (1.68m/s)
Wall	Non-slip wall
Outlet	Normal pressure (1 atm)
Interface area	Frozen rotor
Turbine	Wall (double blades)
Turbulence model	k-ω

Grid System and Mesh Refinement Study

Grid generation was carefully conducted to investigate the influence of mesh resolution on simulated turbine performance. The thickness of the near-wall grid layers was considered according to the turbulence model recommendations, as was the aspect ratio of the mesh. A grid sensitivity study was performed to ascertain whether the selected grid density was of sufficient resolution and to minimise spatial discretization errors. The total number of elements of the original mesh was halved and doubled to generate additional meshes. Figures 4 and 5 show grid dependence study compared to experimental data [9] at a tip speed ratio of 6.

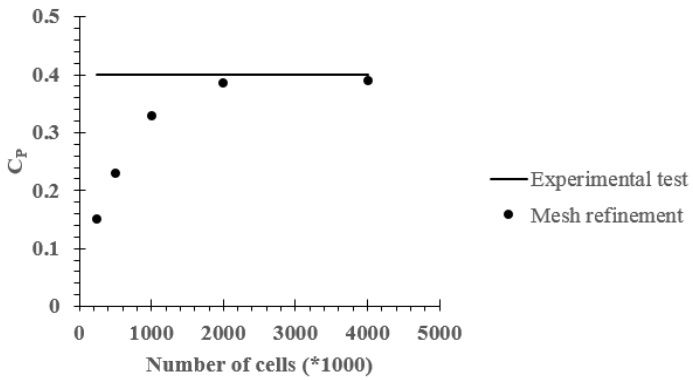

Figure 4: Mesh sensitivity study at $\lambda=6$

As can be seen in Figure 4, the power coefficient converges to the experimental value when the number of cells reaches 2 million. In addition, the difference is below 5% for 2 million cells. Thus, a 2 million cell mesh was chosen for all tip speed ratios.

A layer of prism elements was included around the blade to improve boundary layer modelling and the rest of the area was composed as a tetra-prism mesh.

Result and Discussion

Performance Curve

The power and thrust coefficient curves of the turbine for an inflow current speed of 1.68 m/s are shown in Figures 5 and 6.

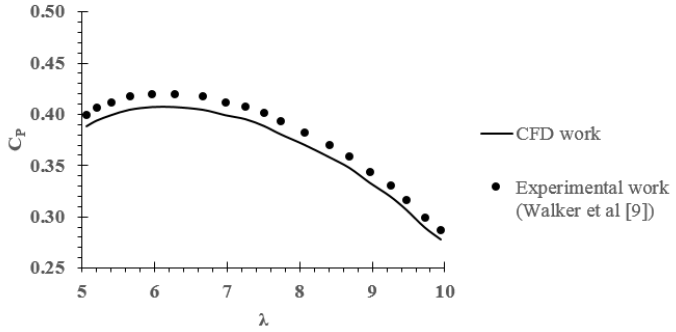

Figure5: Power coefficient

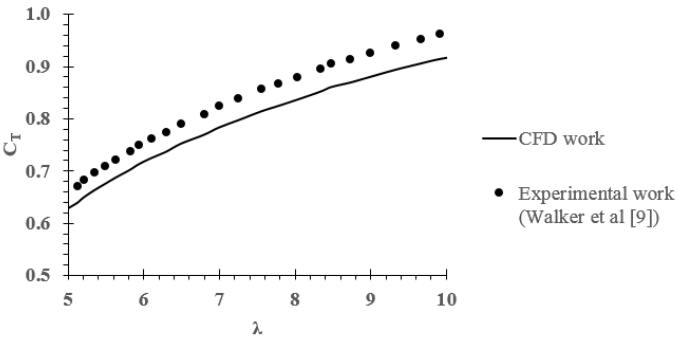

Figure 6: Thrust coefficient

The numerical results agree well with the experimental data. The relative difference for numerical data in thrust coefficient was estimated to be 5%. The maximum value of the power coefficient was calculated as 0.42 for the experimental case [9] and 0.40 for the numerical case. The maximum power coefficient value occurs at a tip speed ratio of 6 in both cases.

Pressure Coefficient Distribution

The pressure distributions of the NACA 63-618 aerofoil at 25%, 50% and 75% of the blade span are plotted in Figures 7, 8 and 9, respectively.

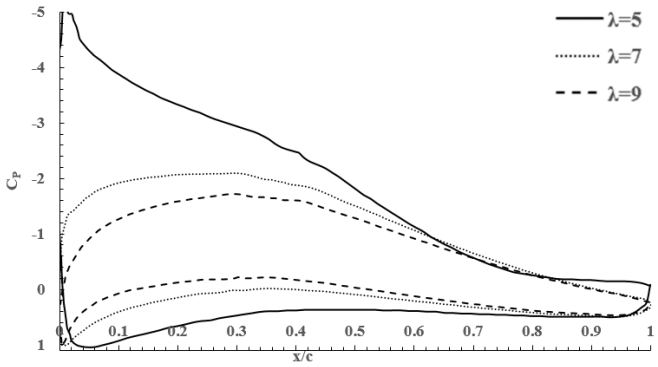

Figure 7: Pressure coefficient of blade at 25% blade span at various tip speed ratios

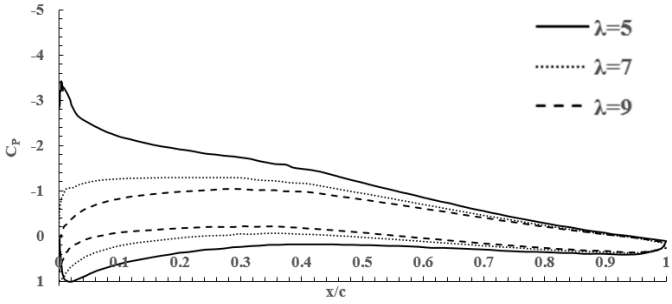

Figure 8: Pressure coefficient of blade at 50% blade span at various tip speed ratios

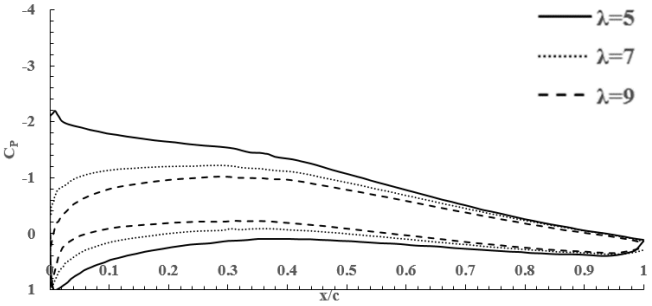

Figure 9: Pressure coefficient of blade at 75% blade span at various tip speed ratios

As shown in these figures, it is clearly seen that the pressure distribution at different blade span is slightly different owing to differences in blade thickness and Reynolds number.

Figure 7 shows the pressure coefficient against the chord-wise position (x/c) at the 25% of blade span. At λ=5, flow separation occurs on the suction side over the region of 0.75<x/c<1 due to the high relative flow angle and strong adverse pressure gradient. As tip speed ratio increases the relative angle of attack is decreased (According to velocity triangle theory, the angle of attack value is functionally related to angle of relative velocity and pitch angle. The section pitch angle is constant for each blade span but the angle of relative velocity is function of tip speed ratio. The angle of relative velocity decreases when tip speed

ratio is increased. Thus, reduction in angle of relative velocity causes decrease in the angle of attack). The adverse pressure gradient at the leading edge part relaxes and the flow remains attached over the whole suction surface.

Figures 8 and 9 show the surface pressure distribution at 50% and 75% radial distance respectively. The pressure distribution for λ=5 represents a strong adverse pressure gradient in the vicinity of the leading edge. At λ=7, the adverse pressure gradient occurs at 0.35 of the chord length and 0.45 for mid-span of blade and 75% of blade span respectively.

The area enclosed between the pressure coefficient curves for each surface is equal to the normal force coefficient of aerofoil (the resultant of the pressure forces acting normal to the chord line) [10]. As expected, the enclosed pressure coefficient area decreases with increasing of tip speed ratio as section blade loading is reduced. It can be noted that an increase in tip speed ratio causes a reduction in normal force coefficient of aerofoil. However, the higher rotational rate increases the normal force magnitude.

Conclusion

A two-bladed horizontal axis tidal power turbine with a NACA63-618 aerofoil cross-section was studied using ANSYS CFX, a commercial CFD code. The k-ω turbulence model was used to investigate incompressible viscous flow past the 3-D tidal turbine blade.

The power coefficient curve shows that the numerical results agree well with the experimental data. At an inflow velocity of 1.68 m/s, the maximum power coefficient was approximately 0.42 and 0.4 for the experimental and numerical cases, respectively. The maximum power coefficient occurred at a tip speed ratio of approximately 6.

The pressure distribution around the aerofoil depends on tip speed ratio. Separation of the suction surface boundary layer is evident at a tip speed ratio value of 5 near the blade root (25% blade span). As tip speed ratio is increased, the adverse pressure gradient is reduced and separation no longer occurs.

The results from this preliminary study will form a useful basis for investigating other factors influencing turbine performance.

References

[1] Lee, J. H. Computational methods for performance analysis of horizontal axis tidal stream turbines, Applied Energy 98, 2010, 512-523.

[2] Pourazam P, Caracoglia L, Lackner M, Modarres-Sadeghi Y. Stochastic analysis of flow-induced dynamic instabilities of wind turbine blades, Wind Eng Industrial Aerodynamics 12(8), 2015, 37-45.

[3] Ghararli K, Johnson DA. Numerical modelling of an S809 aerofoil under dynamic stall, erosion and high reduced frequencies, Apply Energy 93, 2012, 45-52.

[4] Pereira R, Schepers G, Povel MD. Validation of the Beddoes-Leishman dynamic stall model for horizontal axis turbines using MEXICO data. Wind Energy 16(2), 2013, 207-19.

[5] Johari H, Henoch CW, Custodio D, Levshin A. Effects of leading-edge protuberances on aerofoil performance, AIAA 45(11), 2007, 2634-42.

[6] Li Q, Kamada Y, Maeda T, Murata J, Nishida Y. Effect of turbulent inflows on aerofoil performance for a HAWT at low Reynolds numbers (part I: static pressure measurement). Energy 111, 2016, 701-712.

[7] Yu G, Shen X, Zhu X, Du Z. An insight into the separate flow and stall delay for HAT, Renewable Energy 36(1), 2011, 69-76.

[8] Lee HM, Wu Y. An experimental study of stall delay on the blade of a horizontal axis turbine using tomographic particle image velocimetry, Wind Engineering Industrial Aerodynamic 123, 2013, 56-68

[9] Walker J, Flack K, Lust E, Schultz M, Luznik L. Experimental and numerical studies of blade roughness and fouling on marine current turbine performance, Renewable Energy 66, 2014, 257-267.

[10] Houghton E L, Carpenter P W. Aerodynamics for engineering students 2003. Pii:Butterworth Heinemann.